NJC

Accepted Manuscript

This article can be cited before page numbers have been issued, to do this please use: G. Paleti, N. Peddinti, N. Gajula, V. Kadharabenchi, R. R. K.S. and D. R. Burri, *New J. Chem.*, 2019, DOI: 10.1039/C9NJ02287B.

ROYAL SOCIETY OF CHEMISTRY

rsc.li/njc

ROYAL SOCIETY OF CHEMISTRY
View Article Online
DOI: 10.1039/C9NJ02287B

Journal Name

ARTICLE

Direct ethanol condensation to diethyl acetal in vapour phase at atmospheric pressure over CuNPs/ SBA-15 catalysts

Received 00th January 20xx,
Accepted 00th January 20xx

DOI: 10.1039/x0xx00000x

www.rsc.org/

Gidyonu Paleti[ab], Nagaiah Peddinti[a], Naveen Gajula[ab], Vasikerappa Kadharabenchi[ab], Kamaraju Seetha Rama Rao[a] and David Raju Burri*[ab]

Among the biomass valorization technologies, bioethanol production and its selective conversion to diethyl acetal is utmost important to meet the augmenting demand of bio-fuel additives. Direct synthesis of diethyl acetal in a single-step from bioethanol using SBA-15 supported copper nanoparticle (CuNPs/SBA-15) catalysts without using hydrogen acceptors and high pressure has been achieved as an alternative to the age old-two-step process via (i) partial oxidation of ethanol to acetaldehyde and (ii) acetaldehyde acetalization with ethanol. The prepared CuNPs/SBA-15 catalysts with SBA-15 support and copper nitrate (Cu $(NO_3)_2.H_2O$) were characterized by N_2 adsorption, SEM, TEM, XRD, FT-IR, TPD of NH_3, H_2-TPR and N_2O pulse chemisorption techniques and found that the physico-chemical characterestics of these catalysts are responsible for the acceptorless partial oxidation of ethanol to acetaldehyde and its acetalization with ethanol in yielding diethyl acetal with high selectivity.

1. Introduction

Off late, the research focus is towards the production of biomass-derived fuels/fuel additives due to progressive collapse of fossil resources and also to minimize the fossil fuel environmental issues.[1,2] Ethanol, is a major biomass derived platform chemical, obtains through sugar fermentation,[2-4] hence the term bioethanol is more appropriate, which transforms into various high value chemicals such as acetaldehyde, acetic acid, ethylene oxide, ethylene, diethyl ether, ethyl acetate, 1-butene, 1,3-butadiene and diethyl acetal.[5-7] Among these products, diethyl acetal is one of the important derivatives of bioethanol, which is used as a raw material in fragrance and pharmaceutical industries[8-10]and also an important intermediate in production of industrial chemicals (alkyl vinyl ethers).[11] It is also used as organic solvents for cellulose and its derivatives,[11] and also used for the production of polyacetal resins that are employed in electronic components, televisions, cars and printers equipment.[12] Unambiguously, diethyl acetal is a promising green oxygenate useful for diesel blending, which improves the cetane number, reduces the particulate matter and NO_x emissions and also facilitates the combustion without decreasing the ignition quality.[1,14] The industrial production of diethyl acetal is a two-step process[15] via production of acetaldehyde in step-1 from ethanol by oxidative dehydrogenation or hydrolysis of ethylene oxide. The acetaldehyde produced in step-1 is used for the acetalization of ethanol to produce diethyl acetal.

$C_2H_5OH + 1/2O_2 \rightarrow CH_3CHO + H_2O$ ------- (i)
$CH_3CHO + 2C_2H_5OH \rightarrow CH_3CH(OC_2H_5)_2 + H_2O$ ---- (ii)

Production of acetaldehyde (step-1) with high conversions and selectivities under eco-friendly environment is undoubtedly a crucial step. In general, acetaldehyde is being produced by three important methods[16] such as (i) partial oxidation of ethylene, wherein use of an expensive catalyst and high reaction temperature are notable difficulties, (ii) hydration of acetylene, wherein, use of mercury as mercuric complex, which is a toxic material and (iii) dehydrogenation of ethanol to acetaldehyde. This method is somewhat interesting, but ceasing of by-products formation is difficult.

In general, synthesis of acetals is carried out in a homogeneous system in the presence of corrosive liquid inorganic acids such as sulphuric acid, phosphoric acid, p-toluenesulfonic acid (PTSA), triflic acid or dry HCl etc.,[17] which produce significant amount of hazardous waste and in addition involvement of tedious work-up procedure is inevitable.[18] In order to overcome these drawbacks, replacement of homogeneous catalysts by heterogeneous catalysts is the only option. However, there is a limited work is focussed on this issue[19-21] particularly, patent literature.[22]

Direct synthesis or single-step synthesis of acetals from alcohols is an attractive alternative to conventional two-step process and is remain as a challenge to the scientific society,[23] because in this method no need for aldehydes or aldehyde

Address: [a]Catalysis& Fine chemicals Division, Indian Institute of Chemical Technology, Hyderabad- 5000607, INDIA, Fax: +91-40-27160921; Tel: +91-40-27193163; e-mail: david.iict@gov.in
[b]CSIR-Academy of Scientific and Innovative Research(CSIR-AcSIR), New Delhi, India

† Footnotes relating to the title and/or authors should appear here.
Electronic Supplementary Information (ESI) available: [details of any supplementary information available should be included here]. See DOI: 10.1039/x0xx00000x

View Article Online DOI: 10.1039/C9NJ02287B

derivatives. Direct synthesis of symmetric acetals from primary alcohols through a tandem aerobic oxidation–acetalization in presence of a chloride-free $Pd(OAc)_2/Cu(OAc)_2$/p-TsOH bi-functional catalyst without using any solvents under mild conditions (50–80°C, 1–10 atm).[23] But the study is limited to methanol to dimethyl acetal.

A few reports are focussed towards the direct synthesis of higher alcohols to corresponding acetals.[24-27] In one of the reports on direct catalytic conversion of C_5 and C_6 alcohols to corresponding acetals with high conversions and selectivities were claimed in a batch mode reactor using acridine-based ruthenium pincer complex, i.e., RuHCl(A-iPr-PNP)(CO) catalyst at atmospheric pressure, but no reaction of ethanol to diethyl acetal was occurred with the same catalyst.[28]

Coming to ethanol to diethyl acetal, Lloyd reported[29] that the oxidation of ethanol with O_2 using $PdCl_2$ either with $CuCl_2$ or $Cu(NO_3)_2$ as a catalyst, the major products are diethyl acetal, acetaldehyde and ethyl acetate. The formation of both diethyl acetal and acetaldehyde from ethanol was reported in the photocatalytic liquid-phase oxidation over silica-supported Nb or Ti oxides, Re, Ru catalysts and also oxidation by H_2O_2 by Fe(III) complexes.[24-26,30] Through photocatalytic acceptorless dehydrogenation coupling process the conversion of ethanol (<30%) to diethyl acetal (>99% selectivity) over supported titania noble metal catalysts was reported.[31-33]

In the gas-phase selective oxidation of ethanol to diethyl acetal as a main product only 2 papers and 1 patent was reported.[5,15,34] Liu et.al.,[15,34] studied the gas-phase selective oxidative conversion of ethanol on RuO_2/SnO_2, ZrO_2, TiO_2, Al_2O_3, SiO_2 catalysts and claimed the high selectivity (>99%) on RuO_2/SiO_2 and RuO_2/TiO_2 catalysts. Thavornprasert et.al.,[5] reported that the single-step gas-phase selective oxidation of ethanol to diethyl acetal over rhenium(Re) catalysts supported on TiO_2 and amorphous Mo-based catalysts and claimed that these catalysts are highly active, which is the best productivity ever reported so far in the literature.

According to available literature, most of the catalysts used for acetalization are homogeneous, which require long reaction time, harsh reaction conditions, stoichiometric amount of metallic reagents. Most of the heterogeneous catalysts for acetalization are noble metal based, which are unambiguously highly expensive compared to base metals like Ni and Cu. Copper is abundant, cheap and versatile metal. Its chemistry is extremely rich due to its ease of accessing different oxidation states such as Cu^0, Cu^{1+}, Cu^{2+} and Cu^{3+}. Depending on its oxidation state, the copper metal can efficiently catalyse the organic reactions through either one-electron or two-electron mechanisms. Apart from its above cited advantages, copper is found to be one the prominent metal for the selective formation of acetaldehyde (crucial intermediate in acetalization) from ethanol in the non-oxidative method.[35, 36]

Santa Barbara Amorphous (SBA-15) is a two-dimensional (2D) hexagonal silica material having exclusive, imperative and adaptable properties like large surface area, huge pore volume, thick pore wall and ordered mesoporocity was discovered by Zhao *et.al.*[37] Using SBA-15 as a support our group published several articles. Particularly, SBA-15 supported metal/metal nanoparticle catalysts including Cu/SBA-15 and CuNPs/SBA-15 catalysts for various organic transformations.[38-42]

From the above mentioned literature, design and development of suitable solid catalysts for direct synthesis of diethyl acetal from ethanol that are usable under environmentally acceptable and economically viable conditions with improved conversion of ethanol and selectivity of diethyl acetal is present requirement. Herein, an attempt is made to prepare a hexagonally ordered mesoporous CuNPs /SBA-15 bifunctional catalyst that can be operated in a gas phase continuous mode adoptable to ethanol to diethyl acetal reaction. The detailed catalyst preparation, characterization and catalytic application with respect to ethanol to diethyl acetal including optimization of reaction parameters are delineated.

2. Experimental

Catalyst preparation

All the chemicals and the P123 structure directing agent (SDA) were obtained commercially and used without further purification. The SBA-15 silica support was synthesized under hydrothermal acidic conditions using triblock co-polymer (P123) as SDA and tetraethyl orthosilicate (TEOS) for silica source in accordance with the original report of Zhao *et.al*.[36] and our previous publications.[38-42] Prior to prepare CuNPs/SBA-15 catalysts, the SBA-15 support was dried at 120 °C for 6 h. The requisite amounts of aqueous Cu $(NO_3)_2.3H_2O$ solution likely to be around 10, 15, 20, 25 and 30 wt% as Cu metal were impregnated. These catalyst samples were dried at 100 °C for 12 h and calcined at 450 °C for 6 h. A portion of each catalyst was reduced at 280 °C for 3 h in the flow of H_2 gas using a fixed bed reactor and denoted as XCuNPs/SBA-15, where X denotes the percentage loading of Cu metal nanoparticles by weight.

Catalyst Characterization

The amount of copper present in each catalyst sample was calculated by ICP-OES (M/s. Thermo Scientific iCAP6500 DU) by dissolving the CuNPs/SBA-15 catalyst samples in aquaregia with a few drops of HF (hydrofluoric acid). To investigate the mesoporous structural ordering of CuNPs/SBA-15 catalysts, X-ray diffraction (XRD) patterns were recorded at room temperature using a Rigaku, Multiflex, diffractometer with a nickel filtered Cu$K\alpha$ radiation of wave length 0.15418 nm at a power of 40 kW and a current of 100 mA in the 2θ range of 0.5–5°. To verify the structural characteristics of copper in CuNPs/SBA-15 catalysts, the samples were recorded in the 2θ range of 10–80°. The crystallite size estimations were made by Scherrer equation, considering the most intense metallic copper reflection (111) that appears at a 2θ = 43.48°. N_2 adsorption–desorption isotherms were recorded for calcined catalysts using a Tristar 3000 V 6.08A instrument (M/S

Micromeritics Instruments Corporation, USA) at -196 °C. The CuNPs/SBA-15 samples were outgassed at 300 °C for 4 h prior to measurement. BET method was used to calculate the surface areas from N_2 quantity adsorbed at -196 °C. BJH method was used to calculate the pore-size distribution considering the desorption branch of the isotherm. The pore volume was taken at a relative pressure P/P_0 = 0.989 (single point). FT–IR patterns were recorded on a spectrum GX spectrometer (M/s. Perkin-Elmer, Germany) in the scan range of 4000–400 cm^{-1}. Temperature programmed reduction (TPR) studies of all the calcined CuNPs/SBA-15 catalysts were performed on a home-made TPR system that consists of a quartz reactor, temperature programmer, thermocouple and a GC (GC-17A with TCD (M/s. Shimadzu, Japan) with a thermal conductivity detector connected to the outlet of the reactor. About 50 mg of the catalyst sample was placed at the centre of the quartz and heated linearly at a rate of 5 °C min^{-1} from room temperature to 700 °C and isothermal conditions were maintained for 30 min at 700 °C, while passing the 11% H_2 in argon gas. In between the out let of the reactor and GC, a molecular sieve trap was placed to remove the moisture. The TPR profiles were recorded by the connected GC. The acid site distributions were obtained from temperature programmed desorption (TPD) of ammonia. Approximately, 50 mg of catalyst sample loaded in a sample tube was pre-treated in a flow of helium at 300 °C for 30 min. Subsequently, the catalyst sample was saturated with 10% NH_3/He gas mixture at 80 °C for 30 min. After completion of saturation with NH_3, helium was allowed to flow for 30 min at 100 °C for the removal of physisorbed NH_3. Helium gas flow was continued while increasing the temperature to 800 °C at a ramp of 10 °C min^{-1} and the desorbed NH_3 was monitored with on-line GC equipped with TCD using standard GC software. FT-IR spectra of pyridine adsorbed catalysts were recorded by ex-situ method on a Spectrum GX spectrometer (M/s. Perkin–Elmer, Germany) at room temperature. 10 mg of the each catalyst was oven dried at 100 °C for 1 h. To this oven dried sample, 0.1 ml of pyridine was added, followed by vacuum drying at 120 °C for 1 h to remove the physisorbed pyridine. Later, the samples were finely ground and dispersed in KBr (1:100 ratio) and made into a pellet. The spectra were collected using 4 cm^{-1} resolution and averaging five scans in the spectral range of 400–4000 cm^{-1}. The morphological studies of catalysts were carried out by scanning electron microscope (M/s. JEOL, Switzerland). TEM images were obtained on a JEM 2000EXII apparatus (M/s. JEOL, Switzerland) operating between 160 to 180 kV. Prior to TEM analysis, the catalyst sample was ultrasonicated in ethanol and a drop of it was placed onto a carbon coated copper grid and evaporated the solvent in an oven at 80 °C for 6 h. The N_2O pulse chemisorption measurements were done on a home-made pulse chemisorption setup. An automatic gas sampling valve and a GC (GC-17A, M/s. Shimadzu Instruments Corporation, Japan) equipped with TCD and Porapak-T column in separating N_2O and N_2 connected at the inlet and outlet respectively. Prior to each experiment the catalyst was reduced in H_2 flow at 280 °C for 3 h. After completion of the reduction, H_2 gas was replaced by helium gas (carrier gas for GC) and the temperature was brought down to room temperature and N_2O gas (6%N_2O in helium) was introduced onto the catalyst in pulses with the help of 6-port valve. It was assumed that the surface Cu metal sites react with N_2O according to the following stoichiometric equation. [43- 45]

$2Cu + N_2O \rightarrow Cu_2O + N_2$

Copper metal surface area (Cu_{SA}) = No. Cu moles g^{-1} x Avogadro number x cross sectional area of copper metal.

Cu cross sectional area = 6.8 x 10^{-20} m^2 Cu $atom^{-1}$

Surface Cu moles = 2x N_2O uptake (mol g_{cat}^{-1}) from stoichiometry

$$\text{Dispersion, \% } \mathbf{D} = \left[\frac{\textbf{No.of surface Cu metal sites}}{\textbf{Total no. of Cu metal sites in catalyst}}\right] \textbf{x 100}$$

Catalytic activity test

The catalytic activity tests were performed in fixed-bed glass down flow reactor (14 mm id and 300 mm length) at atmospheric pressure. For each catalytic run, the reactor was loaded with 0.5 g of the catalyst mixed with same amount of glass beads sandwiched between two quartz wool plugs at the centre of the reactor. Prior to conduct the reaction, the catalyst was reduced for 3 h at 280 °C. The reaction was carried out in the temperature range of 175–275 °C by feeding ethanol with the flow rate of 1 ml h^{-1} (feed pump, M/s. B. Braun, Germany) along with N_2 carrier gas. The product mixture was collected in an ice cooled trap and analysed the product mixture for every 1 h by GC-17A (M/s. Shimadzu Instruments, Japan) equipped with FID and EB–5 capillary column (30 m x 0.53 mm x 5.0 µm). The products were confirmed by GC-MS, (QP-2010, M/s. Shimadzu Instruments, Japan) with MS column (30 m x 0.25 mm x 0.25 µm).

3. Results and discussion

Textural properties of catalysts

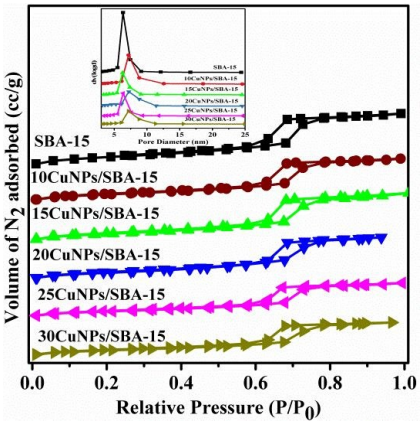

Fig. 1 N_2 adsorption desorption isotherms of CuNPs/SBA-15 catalysts and pore size distribution graph is as inset

View Article Online DOI: 10.1039/C9NJ02387B

The textural properties like BET surface area (S_{BET}), pore volume and pore diameter are presented in Table 1, accordingly, the surface area of the SBA-15 support is 807 m^2g^{-1} which is having the highest surface area compared to all other catalysts prepared from the SBA-15 support. Gradual decrease in surface area with increase in CuNPs loading on SBA-15, revealing the occupancy of some surface area of the support by CuNPs according to loaded CuNPs amount. Since the catalysts were prepared by impregnation technique, the homogeneous $Cu(NO_3)_2.3H_2O$ can reach to either pore surfaces or external surface of the support. The average pore volume of SBA-15 support is 1.35, $cm^3\ g^{-1}$ which is the highest pore volume compared to the pore volume of catalysts prepared from it and further more the pore volumes of catalysts are deceasing with increase in CuNPs loading and are the usual trend. The pore diameters of support and catalysts are more or less constant.

To verify the textural strength of catalysts, N_2 adsorption–desorption isotherms for SBA-15 and CuNPs/SBA-15 catalysts were generated and displayed Fig. 1, which are of type IV and exhibited H1 hysteresis loops, as per IUPAC classification the pore channels are hexagonally ordered similar to that of SBA-15 support, revealing the retention of porous texture of SBA-15 support in all the Cu/SBA-15 catalysts.[38-42] The data presented in Fig. 1 explicitly confirming the robustness of the CuNPs/SBA-15 catalysts. The pore size distribution graph has shown as inset in Fig. 1, wherein the pore sizes of all the catalysts are more or less uniform and are narrowly distributed, symbolizing the pore texture of SBA-15 support.[38-42]

Table 1 Textural property of CuNPs/SBA-15 catalysts

Catalyst	S_{BET} m^2g^{-1}	Pore volume cm^3g^{-1}	Pore diameter nm
SBA-15	807	1.35	6.33
10CuNPs/SBA-15	460	0.81	7.18
15CuNPs/SBA-15	329	0.63	6.27
20CuNPs/SBA-15	305	0.55	7.21
25CuNPs/SBA-15	296	0.53	6.34
30CuNPs/SBA-15	242	0.43	7.17

Structural characteristics by low and wide angle XRD

To assess the structural features of the catalysts including SBA-15 support, low and wide angle XRD patterns were obtained. The wide angle XRD patterns are shown in Fig. 2, wherein low angle XRD patterns are presented as inset. The SBA-15 support exhibited well-resolved diffraction peaks with a sharp peak at about 0.89 and two more weak peaks are observed at about 1.56 and 1.80° on the 2θ scale. Similar kind of XRD patterns were obtained for all the CuNPs/SBA-15 catalysts, but with gradual diminishing in peak intensity with increasing CuNPs loading on the SBA-15 support. On the whole, appearance of diffraction peaks of (100), (110) and (200) planes even in the XRD pattern of 30CuNPs/SBA-15 catalyst, elucidating the presence hexagonally ordered mesoporous structure in all the catalysts. [38-42] The wide angle XRD patterns of all the CuNPs/SBA-15 catalysts (Fig. 2), exhibiting a strong diffraction peak at 2θ = 43.48° followed by two more intense diffraction peaks at 50.5° and 74.1° characteristic of Cu^0 (JCPDS 04-0836), which indicates that the presence of metallic Cu in all the catalysts.

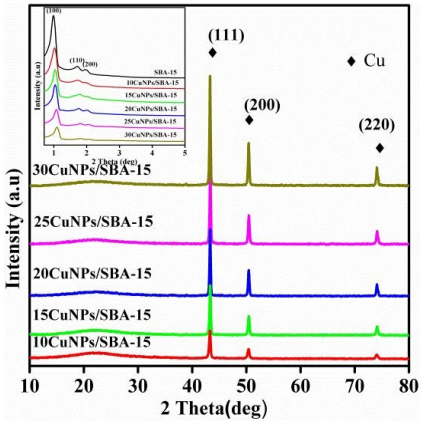

Fig. 2 XRD patterns of reduced CuNPs/SBA-15 catalysts and low angle XRD graph is shown as inset

Additionally, a broad hump is observed in all the patterns of catalysts at around 22°, which corresponds to amorphous silica of SBA-15 support. The crystallite sizes are marginally increased with increase in CuNPs loading on SBA-15 support (Table 2).

Table 2 Catalyst composition and crystallite size from XRD

Catalyst	CuNPs loading, wt%		[b]Crystallite size nm
	Taken	[a] obtained	
10CuNPs/SBA-15	10	8.7	13.1
15CuNPs/SBA-15	15	14.6	14.1
20CuNPs/SBA-15	20	19.4	15.3
25CuNPs/SBA-15	25	24.6	16.0
30CuNPs/SBA-15	30	29.3	17.7

[a] obtained from ICP-OES, [b] obtained from Scherrer equation

FT-IR analysis

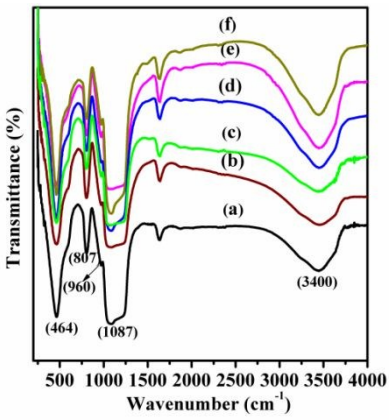

Fig. 3 FT-IR spectra of CuNPs/SBA-15 catalysts (a) SBA-15 support, (b) 10CuNPs/SBA-15, (c) 15CuNPs/SBA-15, (d) 20CuNPs/SBA-15, (e) 25CuNPs/SBA-15 and (f) 30CuNPs/SBA-15

FT-IR spectral analysis was made for all the CuNPs/SBA-15 catalysts including SBA-15 support and the obtained spectra are presented in Fig. 3, accordingly the absorption bands at around 1087, 807 and 464 cm^{-1} are due to the Si- O- Si stretching vibration. The absorption band at around 960 cm^{-1} can be assigned to either Si- OH or Si- O -Si stretching vibrations. The broad absorption band at around 3400 cm^{-1} is due to the presence of surface OH groups with strong hydrogen bonding interactions. The absorption bands at around 660 and 570 cm^{-1} ascribed to Cu- O vibrations in copper oxide lattice.[46]

The nature of acidic sites present in the CuNPs/SBA-15 catalysts were evaluated by performing pyridine adsorbed FT-IR and the corresponding patterns were presented in Fig. 4. Pristine SBA-15 and all CuNPs/SBA-15 catalyst samples show two bands at 1445 and 1597 cm^{-1} which is ascribed to the

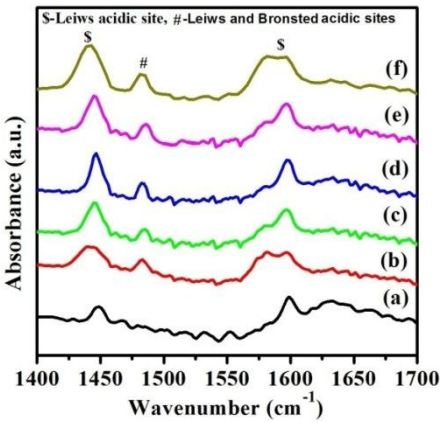

Fig.4 Pyridine adsorbed FT-IR spectra of CuNPs/SBA-15 catalysts (a) SBA-15 support, (b) 10CuNPs/SBA-15, (c) 15CuNPs/SBA-15, (d) 20CuNPs/SBA-15, (e) 25CuNPs/SBA-15 and (f) 30CuNPs/SBA-15

presence of surface Lewis acidic sites coordinated to pyridine. The additional band at 1488 cm^{-1} is a result of combination of Lewis and Bronsted acidic sites.[47-49] It can be observed that the intensities of these bands are increasing with the copper loadings. In the present case all the CuNPs/SBA-15 catalyst samples contain majority of surface Lewis acidic sites compared to Bronsted acidic sites.

Morphological aspects of SBA-15 and 25CuNPs/SBA-15 catalyst

The morphological features of SBA-15 support and 25CuNPs/SBA-15 catalyst were analysed by scanning electron microscope and the acquired SEM images are presented in Fig. 5 (A & B), which are matching with the reported images.[50] TEM images are shown in Fig. 5 (C & D), wherein, existences of array of uniform pore channels are clearly appearing in Figure 5 (D), but not the presence of CuNPs.

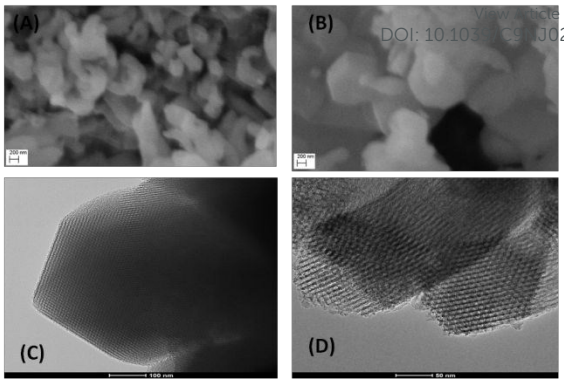

Fig. 5 SEM images of (A) SBA-15, (B) 25CuNPs/SBA-15 catalyst and TEM images of (C) SBA-15, (D) 25CuNPs/SBA-15 catalyst

Reduction behaviour of CuNPs/SBA-15 catalysts

Assessing the reduction behaviour of Cu^{2+} species that supported on SBA-15 has been investigated by a well known and a valid TPR technique. The H_2-TPR profiles of calcined CuNPs/SBA-15 catalysts are displayed in Fig. 6. From the reduction profile of 10Cu/SBA-15 catalyst, only a single peak is observed at 250 °C, which corresponds to the reduction of Cu^{2+} species into metallic Cu. In the case of remaining catalyst 15CuNPs/SBA-15 catalyst two reduction peaks can be observed, where a main reduction peak appeared at 295 °C due to reduction of CuO to Cu^0 or metallic Cu species ($CuO + H_2 \rightarrow Cu + H_2O$) in a single stage and a shoulder peak that appears at 250 °C may be due to reduction of Cu^{1+} species into metallic Cu ($Cu_2O + H_2 \rightarrow 2Cu + H_2O$). Similar reduction behaviour is observed the higher CuNPs loading catalysts. It is clearly seen in the case of 30CuNPs/SBA-15 catalyst, wherein the main reduction peak appearing at 335 °C and a minor peak at 295 °C.

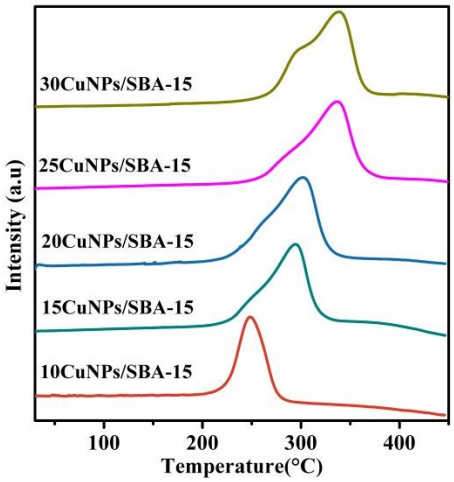

Fig. 6 TPR profiles of calcined CuNPs/SBA-15 catalysts

The results reveal that the interaction between CuO and SBA-15 support increases with CuNPs loading and the CuO species seems to be getting aggregated both in pores and on the

external surface of SBA-15 support and tends towards bulk nature CuO species. The H_2 consumption values of the CuNPs/SBA-15 catalysts are 111.60, 129.28, 209.91, 265.03, and 282.33 µmol g^{-1} for 10, 15, 20, 25 and 30 CuNPs/SBA-15 catalysts, respectively.

Strength of acidic sites by TPD of NH_3 for CuNPs/SBA-15 catalysts

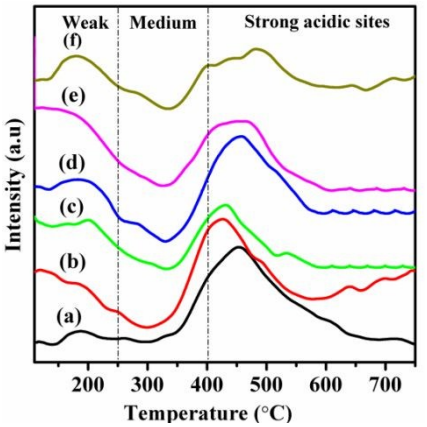

Fig. 7 TPD of NH_3 profiles of CuNPs/SBA-15 catalysts (a) SBA-15 support, (b) 10CuNPs/SBA-15, (c) 15CuNPs/SBA-15, (d) 20CuNPs/SBA-15, (e) 25CuNPs/SBA-15 and (f) 30CuNPs/SBA-15

The NH_3 desorption profiles of SBA-15, Cu/SBA-15 catalysts are depicted in Fig. 7. The acidic sites population can be classified depending upon desorption temperature of ammonia as weak acidic sites (<250 °C), medium (250-400 °C) and strong acidic sites (>400 °C). The desorption signals observed in the TPD profile of pure SBA-15 can be ascribed to the surface hydroxyl groups. All the catalysts except SBA-15, showed a desorption peak in the temperature range of 130-250 °C indicating the weakly chemisorbed NH_3 molecules corresponding to the presence of high amount of weak acidic sites arising from the dispersed copper. Another small peak at around 380 °C could be observed due to the presence of medium acidic sites. From the total acidity values the acidity of the catalysts increases linearly with the copper loadings.

N_2O pulse Chemisorption studies

Table 3 Characteristics of CuNPs/SBA-15 catalysts (N_2O chemisorption)

Catalyst	N_2O uptake µ mol g^{-1}	$^{a}Cu_{SA}$ m^2g^{-1}	$^{b}Cu_{D}$ %	$^{c}Cu_{PS}$ nm
10CuNPs/SBA-15	98	8.1	12.5	8.3
15CuNPs/SBA-15	110	9.1	9.4	11.1
20CuNPs/SBA-15	130	10.7	8.3	12.5
25CuNPs/SBA-15	156	12.9	8.0	13.0
30CuNPs/SBA-15	139	11.5	5.8	17.6

Copper metal ([a] surface area, [b] dispersion and [c] particle size)

To estimate the copper metal surface area, dispersion and particle size N_2O pulse chemisorptions were conducted and acquired data is presented in Table 3. According to Table 3, both N_2O uptake and copper metal surface area of the catalysts from 10CuNPs/SBA-15 to 25CuNPs/SBA-15 catalyst increased and dropped down on 30CuNPs/SBA-15 catalyst and also sudden drop in dispersion and significant increase in particle size is observed for 30CuNPs/SBA-15 catalyst, considering above changes occurred in 30CuNPs/SBA-15 catalyst, it seems that the 25CuNPs/SBA-15 catalyst will be the best catalyst. Deposition of 25 weight% CuNPs on the support with the average particle size of 13nm without adding any surfactant/stabilizers by adopting a facile wet impregnation is unambiguously a significant research improvement in catalyst synthesis

Direct conversion of ethanol to diethyl acetal

The direct conversion of ethanol to diethyl acetal over CuNPs/SBA-15 catalyst in gas phase at atmospheric pressure, wherein one ethanol molecule reduced to acetaldehyde which condensed with other two ethanol molecules forms as diethyl acetal by losing one water molecule as shown in scheme 1.

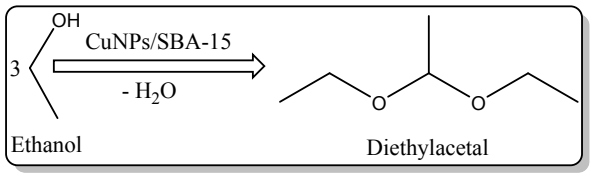

Scheme 1 The reaction scheme for Diethyl acetal formation from ethanol

Influence of CuNPs on direct ethanol conversion to diethyl acetal

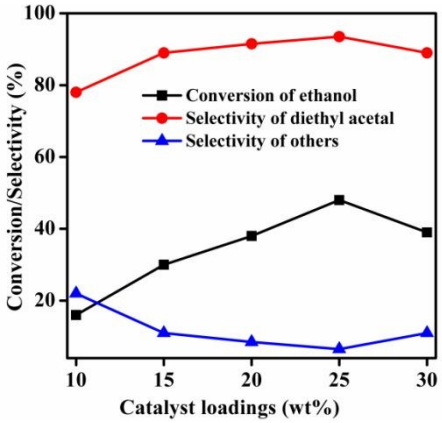

Fig. 8 Effect of CuNPs loading on catalytic activity. Reaction conditions: Temperature: 225 °C, Catalyst weight: 0.5 g, N_2 flow: 30 ml min^{-1}, Feed flow: 1 ml h^{-1}.

To investigate the optimum loading of CuNPs on the SBA-15 support, the direct conversion of ethanol to diethyl acetal was conducted on all the six catalysts (10CuNPs/SBA-15 to 30CuNPs/SBA-15) in the gas-phase at 225 °C in the inert atmosphere using nitrogen gas and the data are displayed in Fig 8, which demonstrate that the increase in conversion of ethanol with increase in CuNPs loading from 10 to 25% is due to increase in the number of active sites available for participating in the reaction. However, the increase in conversion with increase in CuNPs loading from 25 to 30% is marginal, implying that high metal content may lead to agglomeration of CuNPs metal particles and furthermore,

selectivity to diethyl acetal decreased significantly due to simultaneous increase in the selectivity to other product (acetaldehyde, butanol and ethyl acetate).

It can be ascertained that the active sites responsible for the dehydrogenation followed by dehydration of ethanol and formation of other product are different. Among the CuNPs/SBA-15 catalyst series, the 25CuNPs/SBA-15 catalyst exhibited highest activity with 48% conversion of ethanol and 93% selectivity of diethyl acetal. The remaining 7% are acetaldehyde, ethylacetate and butanol, where as Lu et al, reported that the major product is acetaldehyde with selectivity of 68.1% on 10Cu/SBA-15 catalyst. The discrepancy in the catalytic activity may be due to variation in the catalyst preparation, activation and operating conditions.[51] The present results demonstrate that there is a significant influence of the CuNPs loading on the SBA-15 support. It seems that there is a striking balance between the conversion of ethanol and selectivity to diethyl acetal over the 25CuNPs/SBA-15 catalyst. Hence, the best catalyst is 25CuNPs/SBA-15 catalyst with in this catalyst series.

Effect of reaction temperature on activity over 25CuNPs/SBA-15

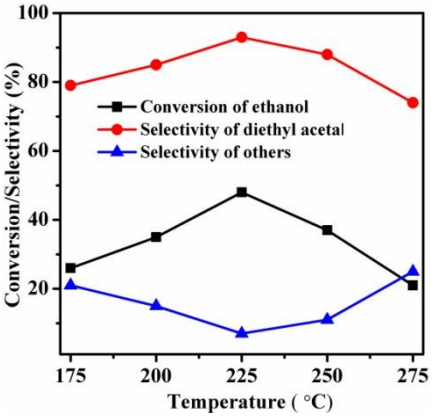

Fig. 9 Effect of reaction temperature on activity over 25CuNPs/SBA-15 Reaction conditions: Catalyst weight: 0.5 g, N_2 flow: 30 ml min^{-1}, Feed flow: 1 ml h^{-1}.

In order to know the effect of reaction temperature on the activity of 25CuNPs/SBA-15, the direct conversion of ethanol was conducted at five different temperatures from 175 to 275 °C (Fig.9). With the increase in reaction temperature from 175 to 225 °C, conversion of ethanol increased from 26% to 48% and selectivity of diethyl acetal increased from 79% to 93%. In other words the yield of diethyl acetal increased from 21% to 45%. i.e., the yield of diethyl acetal at 225 °C is 45%. Beyond the reaction temperature of 225 °C, decrease in ethanol conversion as well as selectivity of diethyl acetal are observed and at the same time selectivity of by-products increased significantly. Since ethanol conversion to acetaldehyde is a primary step, its further conversion to diethyl acetal is an equilibrium reaction, favouring of backward reaction with increased temperatures is a common phenomenon and increment in the selectivity of by-products at higher temperatures is expected.

Time-on-stream (TOS) study on 25CuNPs/SBA-15 catalyst

The TOS study was conducted on 25CuNPs/SBA-15 catalyst at 225 °C for a period 10 h, the conversion of ethanol and selectivity of diethyl acetal are constant at 48% and 93% respectively, revealing the activity of catalyst is stable under the employed reaction conditions (Fig. 10).

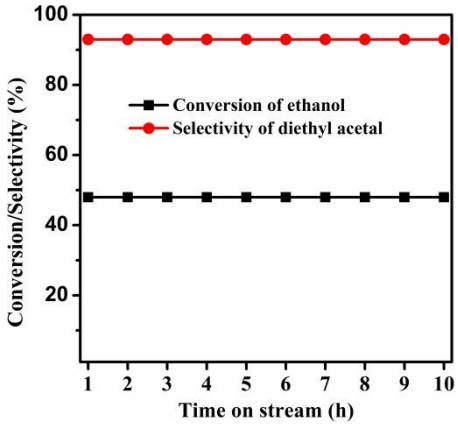

Fig. 10 Time-on-stream activity of 25CuNPs/SBA-15 catalyst. Reaction conditions: Temperature: 225 °C, Catalyst weight: 0.5 g, N_2 flow: 30 ml min^{-1}, Feed flow: 1 ml h^{-1}.

The maximum yield of diethyl acetal is about 45% over 25CuNPs/SBA-15 catalyst at 225 °C in the fixed bed gas phase reactor at atmospheric pressure, which is the highest yield of diethyl acetal so far in the open literature.

In general, acetalization occurs between an aldehyde and alcohol, if any of these two reactants absent, it is hard to expect acetalization product. But, it is possible with alcohols alone by direct coupling over a suitable catalyst and conditions. In-situ formation of an aldehyde via acceptor less dehydrogenation of an alcohol molecule is an essential initial step. According to earlier reports[52] copper metal is capable of dehydrogenating the alcohol to aldehyde even in the absence of acceptors, which is the basis for choosing the copper metal as active component, particularly in the form of nanoparticles, because nanoparticles perform the reaction well compared to bulk copper metal particles. The high activity of 25CuNPs/SBA-15 catalyst is mainly two reasons, (i) unique porous network of SBA-15 (ii) 13 nm sized copper nanoparticles with high copper amount (25wt%). The texture of SBA-15 support is hexagonally ordered pores with uniformly sized mesopores. Each bundle of hexagonally ordered pores of SBA-15 support is expected to act like small copper nanoparticles loaded multi-tubular reactor in the case of smaller CuNPs particles (< 6.34 nm) that are located inner pore walls of SBA-15 support. As reported in the literature the appropriate catalyst for this reaction likely to be bifunctional, which should posses both acidic and redox sites, wherein redox sites enable the partially oxidised redox products like acetaldehyde from ethanol and the acidic sites facilitate condensation.[5] To sum up, 25CuNPs/SBA-15 catalyst with large amount of copper nanoparticles with small particle size (13 nm), uniform dispersion, acidic and redox bi-functional characteristics, ordered mesoporosity, ease of active sites accessibility, confined environment etc., cooperatively facilitated in getting the higher conversion of ethanol (48%) and higher selectivity of diethyl acetal (93%) via single-step

View Article Online
DOI: 10.1039/C9NJ02287B

synthesis or direct synthesis of diethyl acetal from ethanol in the environmentally acceptable vapour phase conditions using a fixed bed reactor.

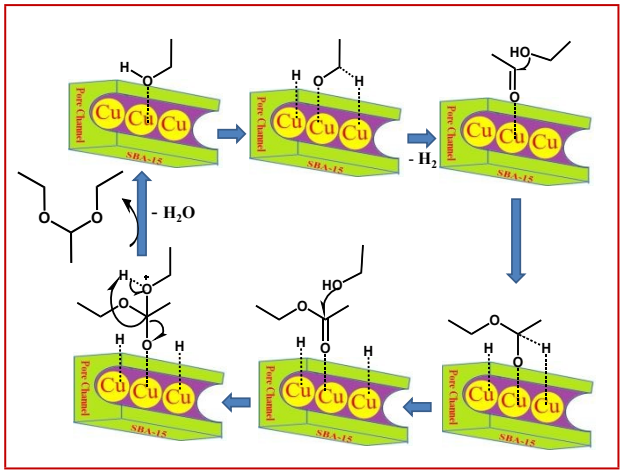

Scheme 2 Single-step synthesis of Diethyl acetal from ethanol over mesoporous SBA-15 supported copper nanoparticle catalysts

The mechanistic aspects of ethanol to Diethyl acetal (Scheme 2) are shown in steps as follows

1. Ethanol adsorbed by the catalyst that leads to oxidative addition of ethanol with Cu^0 to Cu^{2+}.

2. Absorption of α-hydrogen from ethanol and eliminate the H_2 in reductive elimination to form the acetaldehyde.

3. The acetaldehyde which is formed in the second step has highly electronic deficient, the nucleophilic O in the ethanol attacks the electrophilic C in the C=O, breaking the π bond and giving the electrons to the positive O and forms the hemi-acetal.

4. Absorption of hydrogen from α-position of hemi acetal forms the ethyl acetate.

5. The carbonyl carbon in ethyl acetate is somewhat electron deficient, the nucleophilic O in the alcohol attacks the electrophilic C in the C=O, breaking the π bond and giving the electrons to the positive O and forms the oxonium ion intermediate.

6. Finally the oxonium ion rearranged to loss the water molecule and forms the diethyl acetal.

Conclusions

1. SBA-15 supported copper nanoparticle catalysts (CuNPs/SBA-15) up to 30wt% copper nanoparticle loading, <20 nm particle size and hexagonally ordered porous network are prepared.
2. Novel synthesis of diethyl acetal from ethanol over CuNPs/SBA-15 catalysts in a single-step without using aldehyde or aldehyde derivatives, solvents and harmful acids or expensive reagents was achieved.
3. Facile gas-phase operation (25%CuNPs/SBA-15 catalyst) with high conversion of ethanol (48%) and high selectivity of diethyl acetal (93%) was achieved, which are the best results so far, based on the employed reaction conditions.
4. Superior and robust activity of this 25%CuNPs/SBA-15 catalyst can be ascertained from its compatible porous network, confined environment, smaller copper particle size and their ample amount.

There are no conflicts of interest to declare

Acknowledgements

GP, NP and VK are acknowledging the DST, New Delhi, India for granting the research fellowships.

References

1 J. C. Serrano-Ruiz and J. A. Dumesic, Energy Environ. Sci. 2011, **4,** 83.
2 T. Wheeler and J. von Braun, Science, 2013, **341,** 508.
3 M. Neureiter, H. Danner, C. Thomasser, B. Aidi and R. Braun, Appl. Biochem. Biotech., 2002, **98,** 49.
4 O. J. Sanchez and C. A. Cardona, Bioresour. Technol. 2008, **99,** 5270.
5 K.-A. Thavornprasert, B. de la G. de Menorva, M. Capron, J. Gornay, L. Jalowiecki-Duhamel, X. Secordel, S. Cristol, J.-L. Dubois and F. Dumeignil, Biofuels, 2012, **3(1),** 25.
6 S. Hanspal, Z. D .Young, J. T. Prillaman and R. J. Davis, J. Catal., 2017, **352,** 182.
7 C. Angelici, B. M. Weckhuysen and P. C. A. Bruijnincx, ChemSusChem, 2013, **6,** 1595.
8 F. A. J. Meskens, Synthesis 1981, **7,** 501.
9 B. D. Mookherjee, R. W. Trenkle, S. M. Patel and S. M. Brown, US5321006 (1994).
10 M. Kaufhold and M. Del-Chabawi, US5527969 (1996).
11 V. M. T. M. Silva and A. E. Rodrigues, Chem. Eng. Sci.,2001, **56,** 1255.
12 V. M. T. M. Silva and A. E. Rodrigues, AIChE. J., 2005, **51**, 2752.
13 K. Bonhoff, F. Obenaus, Pat DE 2911411 (1980) to Daimler, Benz Germany
14 N. Marshall, Petrochemical Processes, Gulf publishing, Texas, 1989.
15 Liu and E. Iglesia, J. Phys. Chem. B 2005, **109**, 2155.
16 J. McKetta, Encyclopedia of Chemical Processing and Design. Marcel Dekker, Inc. New York, 188, **1**, 114.
17 M. Kaufhold, M. El-Chahawi. Pat. DE 44 04 515 A1 (1995).
18 H. Yang, B. Li and Y. Cui, Synth. Commun., 1993, **28**, 1233.
19 K. Shimizu, E. Hayashi, T. Hatamachi, T. Kodama and Y. Kitatama, Trahedron Lett. 2004, **45**, 5135.
20 Y. J. Kim and R. S. Varma, Tetrahedron Lett. 2005, **46**, 7447.
21 B. C. Ranu, R. Jana and S. Samanta, Adv. Synth. Catal. 2004, **346**, 446.
22 J. Andrade, D. Arntz, M. Kraft and G. Prescher. Pat. DE 34 03 426 A1 (1985), to Degussa AG, Germany.
23 A. C. Bueno, J. A. Goncalves and E. V. Gusevskaya, Appl. Catal. A: Gen., 2007, **329**, 1.
24 T. Tanaka, S. Takenaka, T. Funabiki and S. Yoshida, Chem. Lett. 1994, 809.
25 C. Heitler, D. B. Scaife and B. W. Thompson, J. Chem. Soc. A, 1967, 1409.
26 A. L. Suing, C. R. Dewan, P. S. White and H. H. Thorp, Inorg. Chem. 2000, **39**, 6080.
27 H. Mimoun, DE Patent 1979, 2920678.

View Article Online
DOI: 10.1039/C9NJ02287B

28 Gunanathan, L. J. W. Shimon and D. Milstein, J. Am. Chem. Soc. 2009, **131**, 3146.
29 C W. G. Lloyd, J. Org. Chem. 1967, **32**, 2817.
30 T. Tanaka, S. Takenaka, T. Funabiki and S. Yoshida, Stud. Surf. Sci. Catal. 1994, **90**, 485.
31 H. Zhang, W. Zhang, M. Zhao, P. Yang and Z. Zhu, Chem. Commun., 2017,**53**, 1518.
32 H. Zhang, Z. Zhu, Y. Wu, T. Zhao and L. Li, Green Chem., 2014, **16**, 4076.
33 H. Zhang, Y. Wu, L. Li and Z. Zhu, ChemSusChem, 2015, **8**, 1226.
34 H. Liu, E. Iglesia, 2005, US0059839A1
35 F.-W. Chang, H.-C. Yang, R. L. Selva and W.-Y. Kuo, Appl Catal A Gen, 2006, **304**, 30.
36 R. Prasad, Mater Lett., 2005, **59**, 3945.
37 D. Zhao, J. Feng, Q. Huo, N. Melosh, G. H. Fredrickson, B. F. Chmelka and G. D. Stucky, Science 1998, **179**, 548.
38 N. Anand, K. H. P. Reddy, V. Swapna, K. S. R. Rao and D. R. Burri, Micropor. Mesopor. Mater. 2011, **143**, 132.
39 S. Ganji, S. Mutyala, C. K. P Neeli, K. S. R. Rao and D. R. Burri, RSC Adv., 2013, **3**, 11533.
40 40. C. K. P. Neeli, M. R. Kumar, G Saidulu, K. S. R. Rao and D. R. Burri, J. Chem. Technol. Biotech. 2015, **90**,1657.
41 C. K. P Neeli, V. S. P. Ganjala, V. Vakati, K. S. R. Rao, D. R. Burri, New J. Chem., 2016, **40**, 679.
42 S. Ganji, P. Bukya, V. Vakati, K. S. R. Rao and D. R. Burri, Catal. Sci. Technol. 2013, **3**, 409.
43 P. Nagaiah, M. Venkat Rao, K. Thirupathaiah, V. Venkateshwarlu, D. R. Burri and K. S. Rama Rao, Res. Chem. Intermed. 2018, **44**, 5817.
44 G. Krishna Reddy, K. S. Rama Rao and P. Kanta Rao, Catal. Lett.1999, **59**, 157.
45 J. W. Evans, M. S. Wainwright, A. J. Bridgewater and D. J. Yang, Appl. Catal. 1983, **7**, 75.
46 V. Subbaramaiah, V. C. Srivastava, and Indra Deo Mall, AIChE Journal, 2013, **59(7),** 2577.
47 S. S. Enumula, K S Koppadi, V R B Gurram, D. R. Burri and S. R. R. Kamaraju, Sustainable Energy Fuels, 2017, **1**, 644.
48 X. L. Yang, W. L. Dai, R. Gao and K. Fan, J. Catal., 2007, **249**,278.
49 K. Barbera, P. Lanzafame, A. Pistone, S. Millesi, G. Malandrino, A. Gulino, S. Perathoner and G. Centi, J. Catal., 2015, **323**, 19.
50 M. Kondeboina, S. S. Enumula, V. R. B. Gurram, R. R. Chada, D. R. Burri and S. R. R. Kamaraju, J. Ind. Eng. Chem.,2018, **61,** 227.
51 Q.-N. Wang, L. Shi, and A.-H. Lu, ChemCatChem, 2015,**7**, 2846.
52 R. K. Marella, C. K. P. Neeli, S. R. R. Kamaraju and D. R. Burri, Catal. Sci. Technol., 2012, **2**, 1833.